Design and Development of Low-Cost and High-Efficiency Variable-Speed Drive System With Switched Reluctance Motor

Keunsoo Ha, *Student Member, IEEE*, Cheewoo Lee, *Student Member, IEEE*, Jaehyuck Kim, *Student Member, IEEE*, R. Krishnan, *Fellow, IEEE*, and Seok-Gyu Oh, *Member, IEEE*

***Abstract*—Low-cost switched-reluctance-motor (SRM) drive systems are actively sought for high-efficiency home appliances and power tools. Minimizing the number of switching devices has been in power converters that is the main method to reduce drive costs. Single-switch-per-phase converters have been cost effective due to the compactness of the converter package resulting in a possible reduction in their cost. However, some of the single-switch-per-phase converters have the drawbacks that include higher losses and low-system efficiency. In order to overcome these shortcomings, the choice narrows down to the split ac converter through the quantitative analysis in terms of device ratings, cost, switching losses, conduction losses, and converter efficiency. Simulations to verify the characteristics of the converter circuit and control feasibility are presented. The motor drive is realized with a novel two-phase flux-reversal-free-stator SRM and a split ac converter. The efficiency with various loads is numerically estimated and experimentally compared from the viewpoint of subsystem and system in details. The acoustic noise with no load and full load is also compared. The focus of this paper is to compare the considered split ac converter to the asymmetric converter through experiments and demonstrate that the split ac converter is the most advantageous with respect to cost, efficiency, and acoustic noise.**

***Index Terms*—Acoustic noise, high efficiency, low cost, switched reluctance motor (SRM).**

I. Introduction

THE SEARCH for a lower cost and higher efficiency brushless motor drive has intensified with the advent of variable-speed applications in home appliances and power tools. While a variable-speed motor drive may become acceptable in some appliances, the industry predominantly moves away from brush- and commutator-based machines for reasons of reliability, safety, longevity, and acoustic noise [1]. Hence, the search for a simpler and lower cost brushless motor drive has intensified with the prospective oncoming variable-speed applications. One of the possible electrical machines in low-cost and variable-speed drives is the switched reluctance motor (SRM). SRM drive system is a strong candidate for low-cost variable-speed applications, and that is mainly due to the simple construction of the machine, brushless operation, absence of magnets, and windings on the rotor while still maintaining a relatively high torque density. This makes it potentially a very cost-effective and high-performance drive suitable for many applications. Another key to realize such low-cost motor drive is minimizing the number of switching devices, and one of the cost-effective solutions is using a single-switch-per-phase converters.

Many cost-reducing solutions have been proposed, and almost all have concentrated on minimizing the number of power switches. Single-switch-per-phase converters are most suitable for inexpensive applications due to their relatively low component count and simplicity of the drive system as compared to other well-known converters [2].

The asymmetric converter [3], shown in Fig. 1(a), is a well-known converter that has two power switches and two diodes per phase, resembling the conventional ac motor drives, and the minimum voltage rating of each switch is the dc-link supply voltage. The motor phases are independently controlled. The main disadvantage is the total number of the switches and the diodes which reduces its cost competitiveness, and it is only embraced in high-performance applications.

The single-switch-per-phase configuration [4] is highly cost effective because it contains only one switch per phase. Several topologies in this category have been developed such as bifilar, R-dump, C-dump, and split dc link. Bifilar and R-dump have the drawback of lower system efficiency under high-voltage operation. The split dc-link converter [3], shown in Fig. 1(b), has two equally split capacitors and also requires one switch per phase. This converter, however, has drawbacks of having half the dc supply voltage per phase and voltage asymmetry between the two dc-link capacitors.

In [1], a low-cost four-quadrant brushless motor drive, shown in Fig. 1(c), using a single controllable switch is presented. The cost of this converter is significantly lower due to the reduction of attendant circuits such as gate drives, logic power supplies, and heat sinks. However, it has the disadvantage of low-performance since the main phase winding is controlled using the single controllable switch, and the auxiliary winding

Paper IPCSD-06-116, presented at the 2006 Industry Applications Society Annual Meeting, Tampa, FL, October 8–12, and approved for publication in the IEEE TRANSACTIONS ON INDUSTRY APPLICATIONS by the Industrial Drives Committee of the IEEE Industry Applications Society. Manuscript submitted for review January 15, 2006 and released for publication December 8, 2006.

K. Ha, C. Lee, J. Kim, and R. Krishnan are with the Center for Rapid Transit Systems, The Bradley Department of Electrical and Computer Engineering, Virginia Polytechnic Institute and State University, Blacksburg, VA 24061 USA (e-mail: ksha@vt.edu; cwlee101@vt.edu; marcjkim@vt.edu; kramu@vt.edu).

S.-G. Oh is with the Department of Mechatronics Engineering, Jinju National University, Jinju 660-758, Korea (e-mail: sgoh@inju.ac.kr).

Color versions of one or more of the figures in this paper are available online at http://ieeexplore.ieee.org

Digital Object Identifier 10.1109/TIA.2007.895744

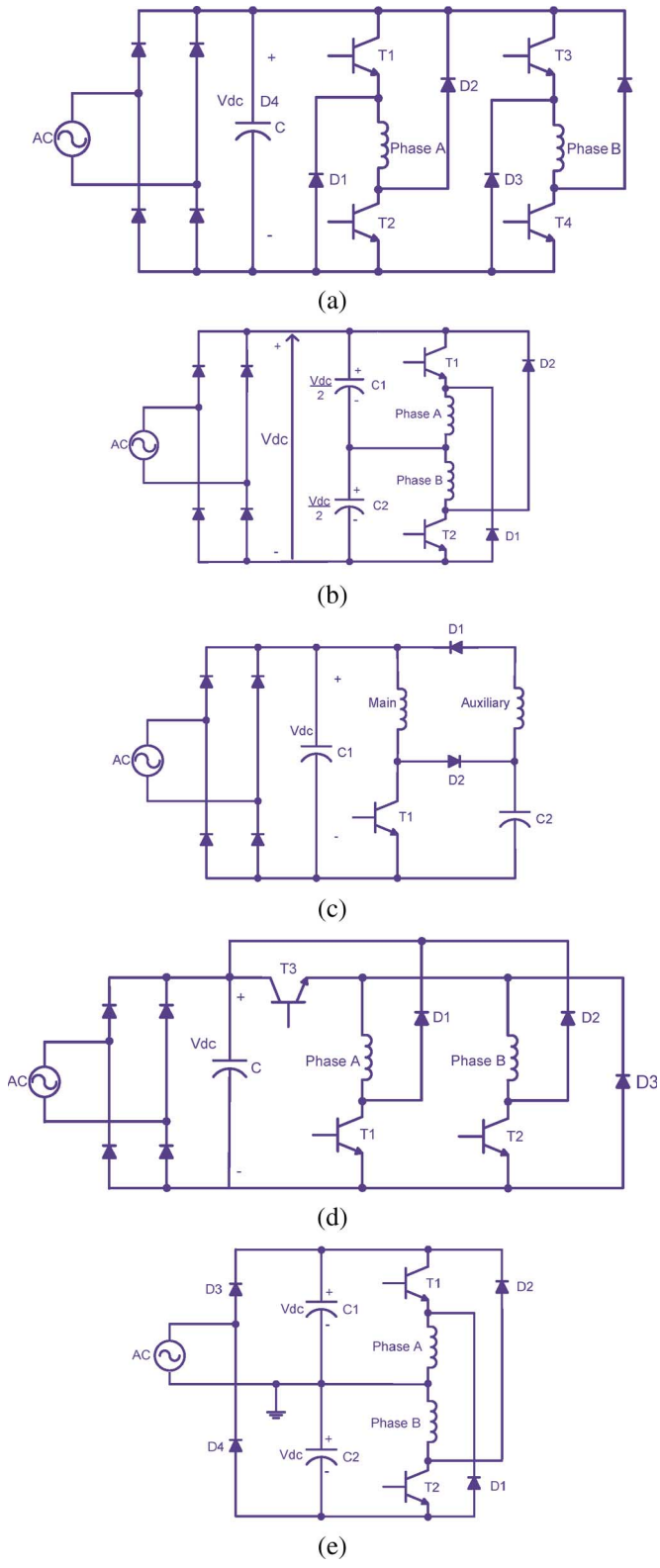

Fig. 1. Converter topologies feasible for two-phase SRMs. (a) Asymmetric bridge converter. (b) Split dc-link converter. (c) Single controllable switch converter. (d) $N+1$ converter. (e) Split ac supply converter.

is used for self-startup, recovering energy from the main phase and for speed reversal.

The $N+1$ switch converter [5] shown in Fig. 1(d), where N is the number of machine phases, uses only one switch per phase with an additional switch shared commonly by all phases. It is intended to minimize the total number of components while achieving a fairly wide range of operating modes: normal conduction, free wheeling, and commutation modes. It has fewer components than an asymmetric converter. In the $N+1$ converter, the phases are not entirely independent, which means that the commutation is sluggish with the common switch conducting.

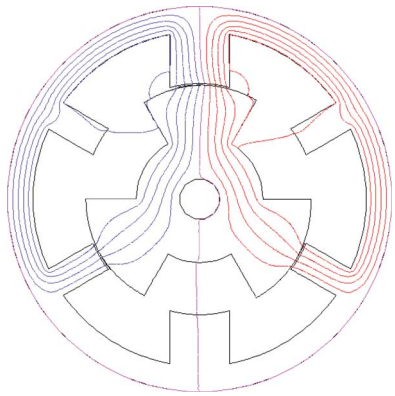

Fig. 2. Finite element flux plot of two-phase SRM.

In order to achieve low cost and high efficiency, the split ac converter [shown in Fig. 1(e)], which has the structure of a single-switch-per-phase converter, is experimentally implemented in the drive system. The half-bridge rectifier splitting ac supply voltage charges one capacitor every ac half cycle, and the capacitor is also charged by storing the energy extracted during the free wheeling and the regeneration of the phase winding producing the torque, resulting in producing significantly greater torque than that is possible from the regular split dc supply converter. In addition, it has an advantage in faster commutation of the phase-winding current.

The experimental verification of the high efficiency and acoustic noise level is achieved using a novel two-phase SRM having the self-starting capability. The novel two-phase flux-reversal-free-stator SRM is described in [6].

This paper is organized as follows. Section II introduces the configuration of the considered two-phase SRM. Section III describes the comparison of the considered converter to the other well-known converters. Section IV presents the operation and structure of the converter. Section V gives the structure of the controller. Based on these developments, its modeling, analysis, and simulation are presented in Section VI. Experimental results are presented both for measuring the efficiency and acoustic noise in Section VII. Conclusions are drawn and presented in Section VIII.

II. Considered Two-Phase SRM [6]

Fig. 2 shows one-phase flux in a two-phase SRM using computer-based finite element analysis. It has one main stator pole and two auxiliary stator poles for one phase. The shape of rotor poles is separated by both a uniform air gap and a nonuniform air gap. The uniform air-gap region is generally formed to minimize reluctance so that inductance can be maximized. The nonuniform air-gap region is necessary to keep

TABLE I
COMPARISON OF CONVERTER LOSSES BETWEEN THE DIFFERENT CONVERTER TOPOLOGIES FOR TWO-PHASE SRM

Type of Losses	Asymmetric		N+1	Split DC	Split AC	Single controllable switch
	Hard	*Soft*				
Convert VA Rating	4VI	4VI	3VI	4VI	4VI	2VI
IGBT Switching	4	2	4	4	4	2
IGBT Conduction	5.3	7.95	5.3	5.3	2.65	2.65
Diode Conduction	3.96	1.65	3.96	3.96	1.98	3.96
Total Converter	**13.26**	**11.60**	**13.26**	**13.26**	**8.63**	**8.61**

increasing the inductance until the uniform air gap generates inductance up to the maximum. These two different air gaps make this motor produce the continuous torque at any rotor position. Another feature is the normal forces that pull in three different directions and prevent ovalization of the stator in two directions and, hence, in the mitigation of stator acceleration that invariably leads to reduced acoustic noise. There is no flux reversal in any part of the stator, and only two thirds of the stator back iron is used. Both of these facts result in lower core losses.

III. COMPARISON OF THE CONSIDERED CONVERTER

Converter design has been one of the main research aspects of SRM drives since performance and cost of the drive are highly affected by the converter configurations. A number of converter topologies suitable for SRM drives have been proposed, implemented, and characterized in literature [1], [2] to facilitate the selection of a proper topology for the given applications. There are several methodologies for converter classification, but all of them give way to the classification by the number of power switching devices. Due to the high cost of power semiconductors and their drive circuits relative to other components in the SRM drive, a large amount of effort has gone into developing the SRM drive converters which utilize the fewest possible number of power switches. Among many converter topologies, five types of configurations, which are shown in Fig. 1, have been found to be feasible for the considered two-phase SRM drive. In this section, both qualitative and quantitative comparisons are presented to find the most appropriate converter configuration in terms of converter efficiency, cost, and performance.

The volt–ampere (VA) rating of the converter is important because it provides a useful measure of the actual power rating of the semiconductor switches that reflects drive cost. The per-unit voltage stress (V) times per-unit current stress (I) that is multiplied by the number of total power switches (N) in the converter gives the converter VA rating $(N \times V \times I)$. Based on this VA rating, the relative converter efficiency can be evaluated by comparing the converter power losses among each different configuration.

The converter power losses can be estimated from each device switching and conduction losses by using the derivation in [7]. The device switching loss is determined by the maximum voltage and current stress, and the device conduction loss is determined by the average current and forward voltage drop from the datasheet under the assumption of the same conditions of control scheme, switching parameters, and torque-speed operation.

For easier comparison between the different converters, normalized power loss is used by setting the discrete insulated-gate-bipolar-transistor (IGBT) switching loss 1 p.u. In the case of hard chopping in the asymmetric converter, the total IGBT switching loss is 4 p.u. since it has four switches for a two-phase SRM. The rationale is applied to estimate the power loss for the remaining converters. Note that all other converters also have 4-p.u. total IGBT loss. The reason is as follows: The $N + 1$ has three switches, and switch T3 in Fig. 1(d) has twice the device switching losses due to the repeated switching operation for every phase. The split dc and split ac converters have half the number of switches when compared to the asymmetric converter, hence, the voltage and current stresses seen by the switch are $[V_{\rm dc}, 2I]$ and $[2V_{\rm dc}, I]$, respectively. Hence, they have the same converter rating $(4VI)$ as the asymmetric converter, resulting in the same total per-unit switching loss (4 p.u.). The single controllable converter also has a $4VI$ rating because of its voltage (2 V) and current $(2I)$ stress, thus, having the same total IGBT switching loss (4 p.u).

The per-unit conduction loss of the discrete IGBT and diode can be determined by the measured average current and ON-state voltage drop from the device datasheet and was found to be 1.33 and 0.99 p.u., respectively, when compared to the discrete IGBT switching loss (1 p.u.). Thus, the total IGBT and diode conduction losses in the asymmetric converter under hard chopping are 5.3 and 3.96 p.u., respectively. In the soft chopping mode, the IGBT switching loss decreases due to the reduced number of switching devices, and the IGBT conduction loss increases to 1.98 p.u. Table I shows the comparison of the total converter losses between the different converter topologies based on the discrete per-unit loss. Likewise, the total IGBT and diode conduction losses for all converters can be determined.

Table I shows the split ac converter that has the lowest power losses resulting in the highest converter efficiency due to its smaller VA rating and fewer number of power switches than any other converter.

TABLE II
OVERALL COMPARISON BETWEEN THE DIFFERENT CONVERTER TOPOLOGIES FOR TWO-PHASE SRM

Features	Asymmetric	N+1	Split DC	Split AC	Single controllable switch
Phase Independence	Yes	No	Partial	Partial	No
Commutation Time	Fast	Slow	Slow	Fast	Slow
Free Wheeling	Yes	Yes	No	No	Yes
Performance	Very Good	Fair	Fair	Good	Low
Number of Rectifier Diodes	4	4	4	2	4
Number of Switches	4	3	2	2	1
Number of Diodes	4	3	2	2	2
Number of Floating Power	5	2	2	2	1
Number of DC Capacitors	1	1	2	2	2
Cost	High	Medium	Low	Low	Lowest
Converter Efficiency	Medium	Low	Low	High	High

Another important factor for selecting the converter topology is overall drive cost which is mainly determined by the number of power semiconductors, isolated gate drivers, passive components, sensors, and control circuits. Table II shows the overall comparison of the considered split ac converter with the other converters in terms of performance, component count, efficiency, and cost.

One of the key components other than power switching devices that affect the overall drive cost is the dc capacitor. As shown in Table II and Fig. 1, the split ac and dc converters require two dc-link capacitors each, and the single controllable switch converter also requires two capacitors; one for the dc link and the other for the energy recovery. Therefore, the cost of the split dc and ac converters could double due to the additional cost of the dc-link capacitors. The increased current-ripple rating increases the capacitance requirement which adds cost to the overall drive.

However, the price reduction that is obtained by the reduced number of power semiconductor devices and their gate-drive circuits still keeps the overall drive cost of the split dc and ac converters lower than the conventional asymmetric converter. Employing appropriate control algorithms to minimize the current ripple can reduce the capacitor size [8]. When comparing the split ac and dc converters, the cost of the split ac is lower due to its lowest number of rectifier diodes.

Although the single controllable switch converter is the least expensive, it is not desirable for our considered drive system due to its low performance and efficiency. The split ac converter has the same power rating as the asymmetric converter but utilizes fewer components, and the total converter loss is the lowest among all the converters, thus, making the split ac converter the most inexpensive and highly efficient configuration.

The classic asymmetric converter is less competitive because of its higher cost; however, due to its high performance and reliability, it has been chosen for performance comparison with the split ac converter.

IV. CONVERTER STRUCTURE

The split ac converter uses a single-switch per phase. Phase A is energized by turning ON switch $T1$. The current can be circulated through T1, phase A, and capacitor $C1$. When T1 is turned OFF, the current will continue to flow through phase A, capacitor $C2$, and diode D_1. In the same mode, capacitor $C2$ is charged, and the stored energy in phase A is depleted quickly. $C2$ would be further recharged by the ac supply if the ac supply voltage were able to forward the bias diode $D2$. Similar operation follows for the excitation and the commutation of phase B. The phase voltage is $V_{\rm dc}$ when $T1$ is ON, and when it is turned OFF with a current present in phase A, the phase voltage is $-V_{\rm dc}$. Therefore, the voltage available to energize and de-energize the phase windings is two times greater than the split dc supply converter. The energy transferring from one phase winding during the turn-OFF instant of current control and commutation provides the energy to force the current through the next phase winding. Instead of the two low-capacitance film capacitors [8], two electrolytic capacitors are used in order to maintain the stable dc-link voltage and provide a sufficient positive torque under the full load condition and low-speed operation.

V. CONTROLLER STRUCTURE

A block diagram of the drive-system control is shown in Fig. 3. Position feedback is needed to synchronize the current flow, with respect to the rotor position, in order to generate the desired motoring torque. It is also required to compute the rotor angular velocity, which is compared with the desired velocity. The soft start block receives the velocity commands at startup

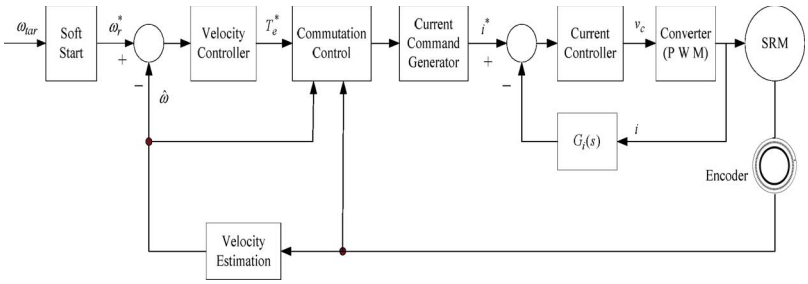

Fig. 3. Drive-system control block diagram.

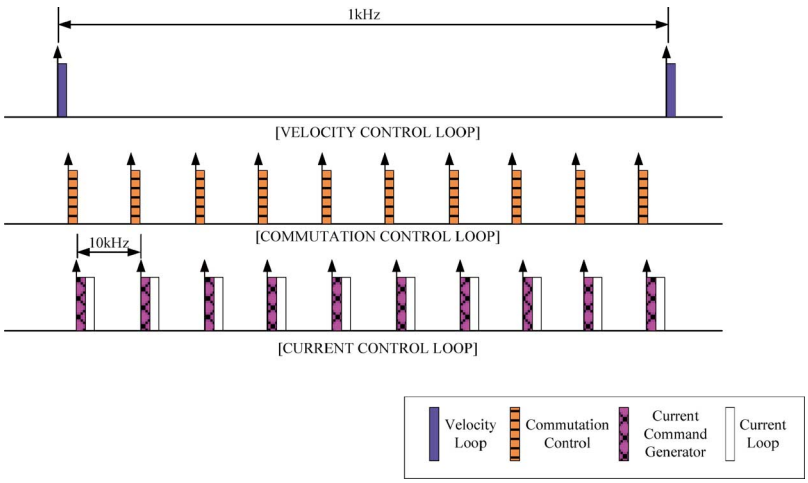

Fig. 4. Timing diagram of the speed controller.

and applies the necessary sequence of commands to each control loop to achieve the new target velocity. After SRM has settled to a new target speed, the soft start loop is encountering its wait state. In this state, it continuously checks if a new target velocity has arrived at the analog-to-digital-converter channel. If a new target speed arrives, the soft start loop shifts into its soft start state. Depending upon whether the new target velocity is above or below the current velocity, the soft start loop will either increment or decrement the current velocity command by 1 r/min every 1 ms. A closed loop velocity controller with a PI control law determines the torque required to bring the motor velocity to the command value at a certain load. A commutation algorithm determines the excitation and commutation logic with respect to the present velocity, and the torque command is eventually converted into a set of phase current commands. The current in an SRM phase winding is directly measured with a current sensor. The measured current is compared with the current command, forming an error signal. The current error is compensated via a PI control law and an appropriate pulsewidth modulation (PWM) control action is taken.

As shown in Fig. 4, the commutation control, the current command generator, and the current control loop are executed at 10 kHz. Because of their lower bandwidth requirements, the velocity control loop is performed at 1 kHz.

VI. Simulations

In order to verify the feasibility of the drive system, it was modeled, simulated, and analyzed. For the controller, a standard modeling procedure given in [3] was used. From finite element analysis of the motor, discrete data sets of 3-D relationships between inductance versus current versus position and torque versus current versus position can be obtained. By using the cubic spline interpolation, the flux linkages and the electromagnetic torque for any rotor position and excitation current can be retrieved [3]. Voltage drops and switching transients of the power electronic devices are negligible compared to the dc-link voltage and mechanical time constant of the motor; therefore, the switching devices are assumed to be ideal. The following system equations combining the converter and motor are derived for each mode of operation that corresponds with the IGBT switching modes.

T1: ON (phase A is energized)

$$\begin{aligned}\nu_{\rm a} &= \nu_{\rm c1} \\ &= R_{\rm a} i_{\rm a} + \frac{d\lambda_{\rm a}}{dt} \\ &= R_{\rm a} i_{\rm a} + L_{\rm a}(\theta, i_{\rm a})\frac{di_{\rm a}}{dt} + i_{\rm a}\frac{dL_{\rm a}(\theta, i_{\rm a})}{d\theta}\omega \end{aligned} \tag{1}$$

$$\nu_{\rm c1} = \frac{1}{C1}\int i_{\rm c1}dt + \nu_{\rm c1}(t_{\rm OFF}), \qquad i_{\rm c1} = -i_{\rm a} \tag{2}$$

$$\lambda_{\rm a} = L_{\rm a}(\theta, i_{\rm a}). \tag{3}$$

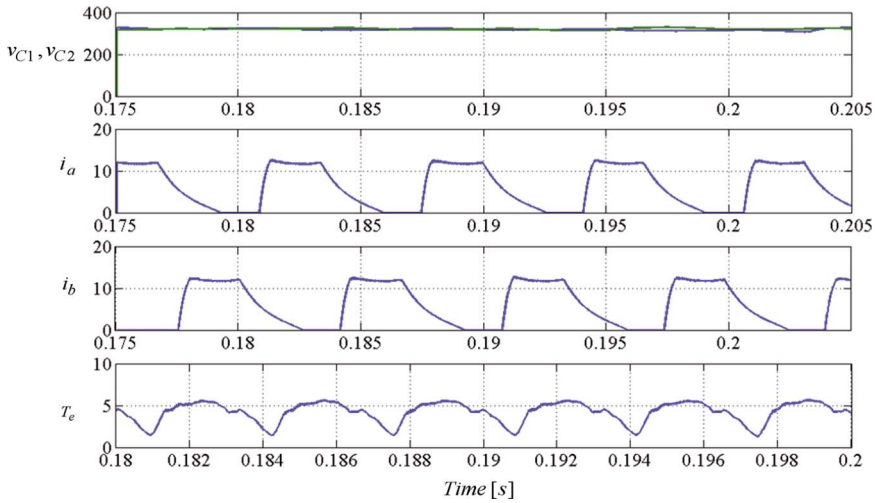

Fig. 5. Simulation of the split ac drive system (scale: Voltage = 200 v/div, current = 10 A/div, and torque = 5 N · m/div).

T1: OFF (phase A is de-energized)

$$\begin{aligned}\nu_{\rm a} &= -\nu_{\rm c2} \\ &= R_{\rm a} i_{\rm a} + \frac{d\lambda_{\rm a}}{dt} \\ &= R_{\rm a} i_{\rm a} + L_{\rm a}(\theta, i_{\rm a})\frac{di_{\rm a}}{dt} + i_{\rm a}\frac{dL_{\rm a}(\theta, i_{\rm a})}{d\theta}\omega \qquad (4)\end{aligned}$$

$$\nu_{\rm c2} = \frac{1}{C2}\int i_{\rm c2}dt + \nu_{\rm c2}(t_{\rm ON}), \qquad i_{\rm c2} = i_{\rm a}. \qquad (5)$$

where $i_{\rm a}$, $i_{\rm c1}$, and $i_{\rm c2}$ are the phase A, capacitor $C1$, and capacitor $C2$ current, respectively; $\nu_{\rm a}$, $\nu_{\rm c1}$, and $\nu_{\rm c2}$ are phase A, capacitor $C1$, and capacitor $C2$ voltage, respectively. $\nu_{\rm c1}(t_{\rm OFF})$ is the capacitor $C1$ voltage at the last time during turn OFF $T1$, and $\nu_{\rm c2}(t_{\rm ON})$ is the capacitor $C2$ voltage at the last time during turn ON $T1$. $R_{\rm a}$, $L_{\rm a}$, and $\lambda_{\rm a}$ are phase A winding resistance, inductance, and flux linkages, respectively. The system equations for phase B can be derived similarly. The motor speed dynamic equation is given as

$$J\frac{d\omega_m}{dt} + B\omega_m = T_{\rm e} - T_{\rm l} \qquad (6)$$

where ω_m, J, and B are the rotor speed, the rotor inertia, and the friction coefficient, respectively. $T_{\rm e}$ is the electromagnetic torque obtained from motor magnetic characteristics as a function of the current and rotor position, and $T_{\rm l}$ is the load torque. Fig. 5 shows the simulation results for operation at 3000 r/min under a load of 4.5 N · m. The upper and lower dc-link capacitor voltages, phase A and B currents, as well as the corresponding electromagnetic torque, are plotted. The voltage to the phase winding is applied in advance by 6°, and the current turn OFF is initiated 30° in advance.

VII. Experimental Results

A. Operation of the Split AC Drive System

The operation of the considered drive system at the rated speed and the full load is shown in Fig. 6. Average phase current is 12 A during the conduction region, and the ripple voltage of the capacitor is 28 V because chopping one phase continuously charged the opposite capacitor. It was caused by the phase energy transfer from the conducting phase to the capacitor during switch turn OFF.

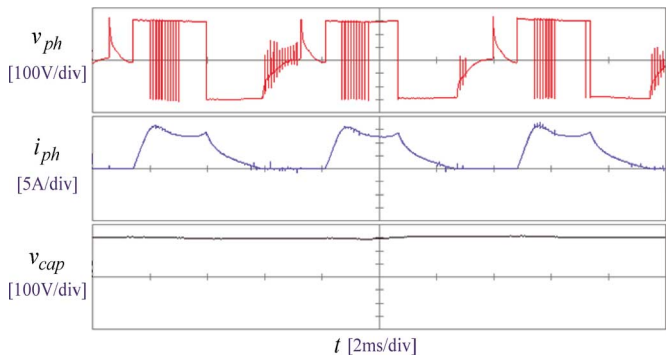

Fig. 6. Operation of the split ac drive system (scale: Phase voltage and capacitor voltage = 100 v/div, phase current = 5 A/div, and time = 2 ms/div).

B. Efficiency

1) Experimental Setup and Measurements: In order to validate the considered drive system, comprehensive sets of experiments were performed. The control algorithm mentioned in Section V was implemented in a 16-b DSP controller, Texas Instrument's TMS320LF2808. Current sensing and feedback was performed using the LA25-NP current transducers manufactured by LEM, Inc. In order to protect the control circuitry, all switches were driven using the optoisolating gate drivers to produce a +15-V gate signal with complete galvanic isolation. It is controlled in the way that the same advanced and conduction angles are used in the considered split ac drive system and the asymmetric drive system in order to compare the efficiency and the acoustic noise level.

The considered split ac drive system and the asymmetric drive system have been tested on a 2.2-hp 3000-r/min two-phase SRM with dc generator as its load shown in Fig. 7. The voltage and current can be measured using a differential

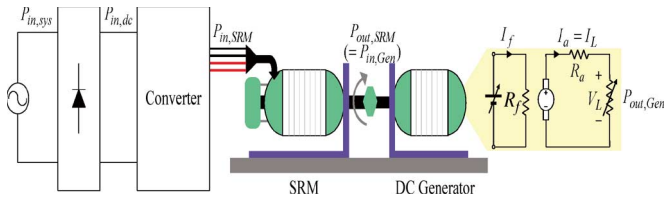

Fig. 7. Experimental setup for measuring efficiency.

TABLE III
RECTIFIER EFFICIENCY AT VARIOUS LOADS (3000 r/min)

Torque [Nm]	Estimations [%]			Measurements [%]		
	Split AC	*Asymmetric*	*Difference*	*Split AC*	*Asymmetric*	*Difference*
1	99.69	99.70	-0.01	98.43	99.30	-0.87
2	99.70	99.68	0.02	99.18	99.49	-0.31
3	99.68	99.67	0.01	98.03	99.50	-1.47
4.5	99.64	99.65	-0.01	98.63	98.39	0.24

probe and a current probe, respectively. The product of the instantaneous voltage and current to obtain the instantaneous power is computed in the oscilloscope. The average power can then be determined. The Appendix describes how to calculate the power and efficiency.

2) Comparisons Between the Estimations and the Measurements: Experimental measurements were performed in order to compare them to the estimations. It can be seen from the following tables that subsystem and system efficiencies for drive system are evaluated by measurement and estimation at various loads.

a) Rectifier efficiency: Rectifier-diode forward drop is 1 V given by the datasheet, and the mean value of dc-link current is used for estimating power losses.

Generally, the asymmetric drive system utilizes the full-bridge rectifier, but in case of the considered split ac drive system, the half bridge rectifier provides the dc bus voltage for each phase winding. The number of diodes for rectifying voltage at the considered split ac drive system is half the number of asymmetric drive system, but it can be seen from Table III that the rectifier losses in the asymmetric drive system are almost the same as that of the split ac drive system although the number of diodes is twice since the average current at each diode for rectifying voltage in the asymmetric drive system is half of the dc-link current.

b) Converter efficiency: Converter power losses dissipated from the switching transients and conduction can be derived analytically by using device characteristics from the datasheet and the measured peak and average currents with the assumption that diode and power switch forward voltage drops are assumed to be constant over various loads.

Although the total number of switching devices is different, two converters have the same switching losses since the voltage rating at the split ac drive system is doubled. However, it can be found from Table IV that switching device's conduction losses and diode losses for the split ac drive system are half that of the asymmetric drive system, and the total converter losses consequently are reduced compared to the asymmetric drive system under full load.

TABLE IV
DRIVE CONVERTER EFFICIENCY AT VARIOUS LOADS (3000 r/min)

Torque [Nm]	Estimations [%]			Measurements [%]		
	Split AC	*Asymmetric*	*Difference*	*Split AC*	*Asymmetric*	*Difference*
1	96.66	95.30	1.30	98.01	95.46	2.55
2	97.59	96.43	1.16	96.54	98.75	-2.21
3	97.90	97.01	0.89	96.23	97.20	-0.97
4.5	97.92	97.22	0.70	97.19	96.86	0.33

TABLE V
MACHINE EFFICIENCY AT VARIOUS LOADS (3000 r/min)

Torque [Nm]	Estimations [%]			Measurements [%]		
	Split AC	*Asymmetric*	*Difference*	*Split AC*	*Asymmetric*	*Difference*
1	63.99	66.09	-2.10	64.55	67.01	-2.46
2	66.10	73.70	-7.60	69.14	71.65	-2.51
3	70.63	75.32	-4.69	74.76	76.18	-1.42
4.5	79.57	79.64	-0.07	81.11	82.45	-1.34

TABLE VI
SYSTEM EFFICIENCY AT VARIOUS LOADS (3000 r/min)

Torque [Nm]	Estimations [%]			Measurements [%]		
	Split AC	*Asymmetric*	*Difference*	*Split AC*	*Asymmetric*	*Difference*
1	61.66	62.89	-1.23	62.27	63.52	-1.25
2	64.31	70.96	-6.65	66.21	70.39	-4.18
3	68.92	72.95	-4.06	70.52	73.67	-3.15
4.5	77.63	77.29	0.34	77.75	78.58	-0.83

c) Machine efficiency: The air-gap power of SRM can be estimated by multiplying the electromagnetic torque and the rotor speed. Table V shows the comparison of efficiency in the machine only for the asymmetric drive system and the considered split ac drive system at various loads while driving at 3000 r/min.

The difference in machine efficiency between the two systems is 2.46% at low load and is decreased to 1.34% at full load. The machine efficiency at the split ac drive system is to a small extent lower than that of the asymmetric drive system at the full load. But, it is always lower since in the free-wheel mode, the terminal voltage is equal to zero, resulting in lower current ripple and lower core loss with the use of soft chopping drive in the asymmetric drive system.

d) Overall system efficiency: Table VI shows the comparison of efficiency in the system aspect, including rectifier, converter, and motor efficiency between the asymmetric drive system and the considered split ac drive system at various loads while driving at 3000 r/min.

The deviation between the two systems is 1.3% at low load and is 3%–4% or so at the middle load, but it is significantly decreased to 0.8% under full load. The split ac drive system produces the efficiency corresponding to that of the asymmetric drive system although the machine efficiency of the split ac drive system is lower than that of the asymmetric drive system. It was caused by the higher efficiency of the rectifier and converter due to the reduction of switching losses and conduction losses of switching devices and diodes.

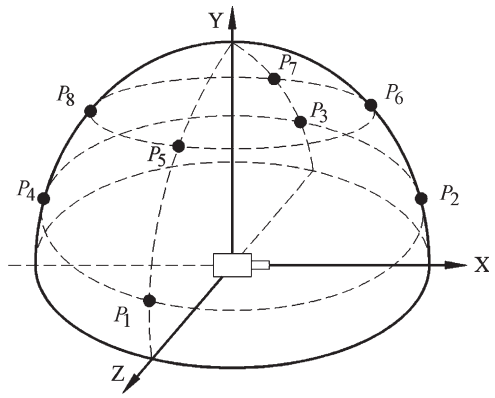

Fig. 8. Locations for measuring the sound-pressure level (radius = 1 m).

C. Acoustic Noise

The acoustic noise has been obtained from the real-time spectrum analyzer. In order to accurately measure the audible noise caused by vibrations in electrical machines, it usually is made in an anechoic chamber after calibrating the measuring equipment and measuring sound pressure at several points. However, an anechoic chamber is not available in the normal laboratory environment, and therefore, measurements can be made in an ordinary large room after measuring the ambient noise.

1) Sound-Pressure Level: As for small motors, the sound-pressure level from the test motor should be measured over a hypothetical hemisphere, centering on the motor and with a radius of 1 m [9], as shown in Fig. 8.

After measuring the sound-pressure levels of eight points with a microphone, each sound-pressure level is averaged in decibels and it can be expressed as

$$\bar{L}_{\mathrm{p}} = 10\log\left\{\frac{1}{n}\left(\sum_{i=1}^{n} 10^{\frac{L_{\mathrm{p},i}}{10}}\right)\right\} \tag{7}$$

where $\overline{L}_{\mathrm{p}}$ is the averaged sound-pressure level in decibels, $L_{\mathrm{p},i}$ is the sound pressure at the ith measurement point, and n is the total number of measurement points.

The ambient noise was 34.80 dB, and it was below the measured acoustic noise from the tested two-phase SRM, and no correction is required for the ambient noise. It can be seen from Table VII for no load and Table VIII for full load that the acoustic noise from the considered split ac drive system is slightly lower than the asymmetric drive system, and it produces a reasonably quiet operation.

2) Frequency Spectrum: Figs. 9 and 10 show that the frequency spectra of the acoustic noise are measured from the considered split ac drive system and the asymmetric drive system. The frequency spectra throughout the eight locations of point were found to have very similar pattern, and a measurement at P2 location is taken for illustration.

The frequency component at 160 Hz is due to the frequency of the phase current at 3000 r/min, and the noise level of the split ac drive system is close to that of the asymmetric drive system. The frequency spectra also show a frequency component at 10 kHz, which is the PWM frequency of the phase current. The noise level of the split ac drive system is 2 dB greater due to the hard chopping drive. The peak component at the frequency spectrum can be found at 800 Hz, and this frequency coincides with five times the phase frequency. It is referred that vibration is maximum when the natural frequency of the stator pole coincides with the odd times the phase frequency [10].

TABLE VII
MEASURED SOUND-PRESSURE LEVEL (NO LOAD)

Location of point	Split AC [dB]	Asymmetric [dB]
P1	40.00	41.30
P2	42.50	45.50
P3	42.40	41.80
P4	39.00	38.00
P5	41.20	39.70
P6	44.30	44.30
P7	42.80	42.50
P8	42.80	42.80
$\overline{L}_p$	**42.15**	**42.54**

TABLE VIII
MEASURED SOUND-PRESSURE LEVEL (FULL LOAD, 4.5 N · m)

Location of point	Split AC [dB]	Asymmetric [dB]
P1	62.90	62.70
P2	63.00	63.70
P3	64.60	61.10
P4	60.80	62.30
P5	60.50	63.80
P6	59.40	61.80
P7	61.80	61.90
P8	64.20	62.30
$\overline{L}_p$	**62.48**	**62.54**

VIII. CONCLUSION

This paper presented a split ac drive system for a novel two-phase flux-reversal-free-stator SRM, and it has a single-switch-per-phase topology. Its performance has been theoretically compared to several types of converter topologies and experimentally compared to an asymmetric converter. It has been analyzed with the system dynamic equations and simulated in order to validate the performance of the split ac converter circuit. Although the efficiency of the machine with the split ac drive system is lower than the asymmetric drive system, the overall system efficiency is very close to the asymmetric drive system due to the better efficiency in rectifier and converter. Subsystem and system efficiency are estimated and measured at various loads, and they are reasonable and acceptable. The acoustic noise spectrum of the split ac drive system has slightly lower average sound-pressure level than the asymmetric drive system. The proposed split ac drive system is a strong contender to be a low-cost motor drive system with a single-switch per

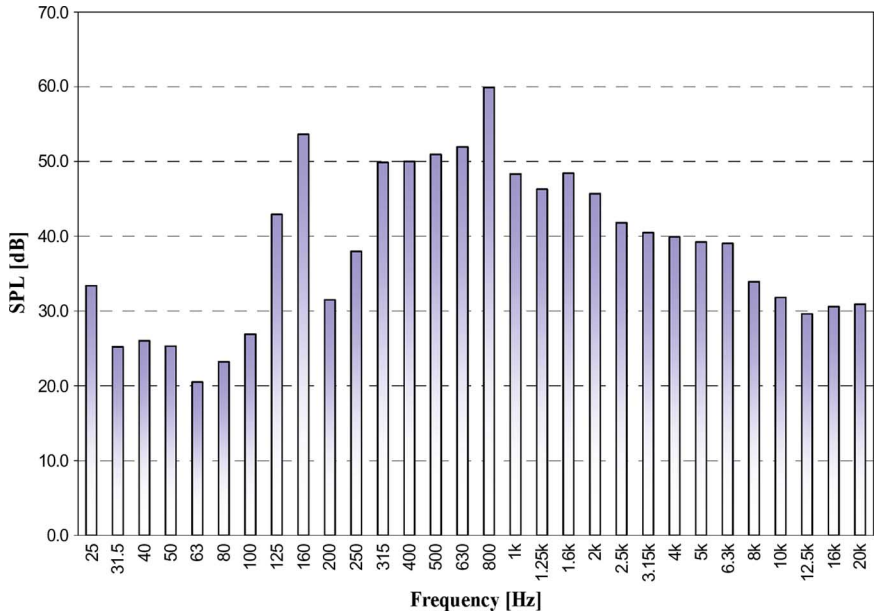

Fig. 9. Frequency spectrum of acoustic noise at the split ac drive system while driving at 3000 r/min and the full load.

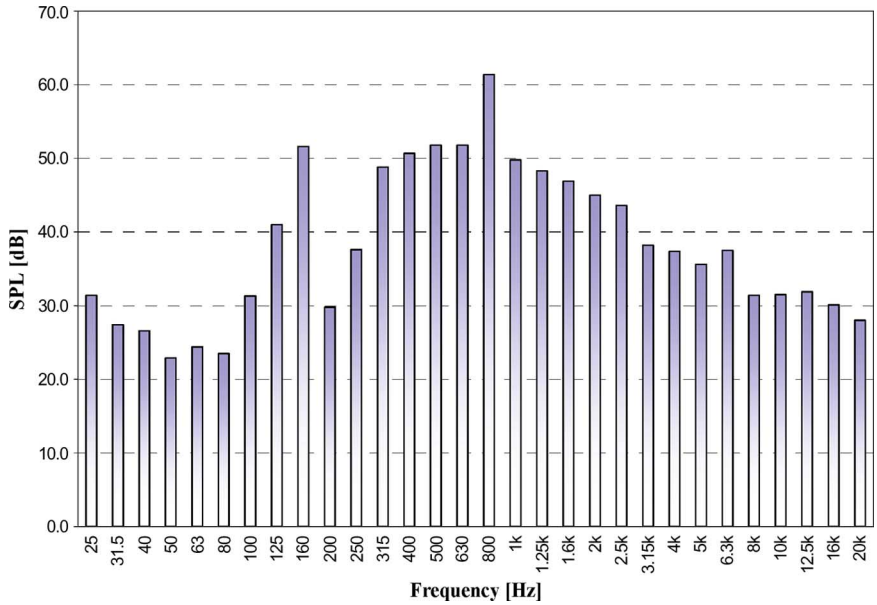

Fig. 10. Frequency spectrum of acoustic noise at the asymmetric drive system while driving at 3000 r/min and the full load.

phase having comparable efficiency and acoustic noise level as an asymmetric drive system under full load.

APPENDIX
CALCULATION OF THE OUTPUT POWER OF SRM

The losses of dc generator, including the copper losses, mechanical losses, core losses, stray losses, and brush contact losses, can be calculated in advance, and based on these losses, the output power of SRM can be calculated.

1) Copper Losses (in Case of Separately Excited Field):

$$P_{\text{copper}} = I_{\text{a}}^2 \cdot R_{\text{a}}. \tag{8}$$

The change in resistance of the armature due to temperature and skin effect has to be considered in order to calculate the accurate copper losses in the dc generator. Improper value of resistance can lead to the reduction of the input power of dc generator, resulting in the reduction of the output of the tested drive system. Temperature measurements are made right after driving, and resistor values for copper at any temperature other than the standard temperature (usually specified at 20 °C) are measured through the following formula [11]:

$$R = R_{\text{ref}} \left[1 + \alpha \cdot (T - T_{\text{ref}})\right] \tag{9}$$

where R is the resistance at temperature T, R_{ref} is the resistance at reference temperature T_{ref}, α is 0.004041, which means the temperature coefficient of resistance for copper, and T is temperature in degree Celsius. Skin effect can be neglected

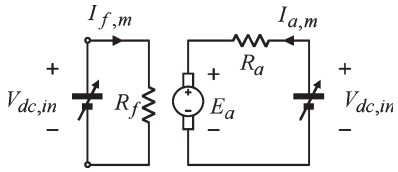

Fig. 11. Circuitry for measuring mechanical and core losses.

since the frequency of dc generator at the rated speed is 100 Hz, and the ac/dc resistance ratio is unity.

2) Mechanical Losses and Core Losses: These two losses can be calculated while driving a dc generator as a dc motor at no load. The output power of dc motor is ideally zero, and all of the input power turn into losses (Fig. 11).

The copper losses in the field and the armature circuits at no load are given as

$$P_{\text{copper},m} = I_{f,m}^2 \cdot R_f + I_{a,m}^2 \cdot R_{\text{a}}. \tag{10}$$

The remaining portion of the input power must be rotational losses of the motor, which is the summation of mechanical losses and core losses. Hence, the rotational losses with respect to speed are expressed as

$$\begin{aligned} P_{\text{mech}} + P_{\text{core}} &= P_{\text{in},m} - P_{\text{copper},m} \\ &= V_{\text{dc,in}} \cdot (I_{a,m} + I_{f,m}) - P_{\text{copper},m}. \end{aligned} \tag{11}$$

3) Stray Losses: It is noted that the stray losses are the miscellaneous losses associated with mainly electromagnetic radiation, and they can be assumed generally to be 0.5% of the full load power

$$P_{\text{stray}} = 0.005 \times P_{\text{out,Gen}}. \tag{12}$$

4) Brush Contact Losses [12]: There is an electric power loss in the brushes that make with the commutator. The potential difference occurs between the commutator surface and the brush material close to the brush contact surface. This potential difference varies nonlinearly with the current density, and the total potential difference across brushes is 1.8 V under the full load in this machine, and it causes the reduction of 1%–2% of the machine and overall system efficiency

$$P_{\text{brush}} = V_{\text{brush}} \times I_{\text{a}}. \tag{13}$$

5) Output Power of DC Generator: It equals to the load voltage multiplied by the load current in the dc generator

$$P_{\text{out,Gen}} = V_L \cdot I_L. \tag{14}$$

6) Output Power of SRM: Consequently, based on the beforehand calculated losses and the output power, the total input power of dc generator corresponds to the output power of the tested drive system

$$P_{\text{out,SRM}} = P_{\text{in,Gen}} = (8) + (11) + (12) + (13) + (14). \tag{15}$$

7) Rectifier Efficiency: It can be found from Fig. 7 that the rectifier efficiency is given as

$$\eta_{\text{rec}} = \frac{P_{\text{in,dc}}}{P_{\text{in,sys}}}. \tag{16}$$

8) Converter Efficiency: It can be found from Fig. 7 that the converter efficiency is given as

$$\eta_{\text{conv}} = \frac{P_{\text{in,SRM}}}{P_{\text{in,dc}}}. \tag{17}$$

9) Machine Efficiency: It can be found from Fig. 7 that the machine efficiency is given as

$$\eta_{\text{SRM}} = \frac{P_{\text{out,SRM}}}{P_{\text{in,SRM}}}. \tag{18}$$

10) System Efficiency: It can be found from Fig. 7 that the overall system efficiency is given as

$$\eta_{\text{sys}} = \frac{P_{\text{out,SRM}}}{P_{\text{in,sys}}} = \eta_{\text{rec}} \cdot \eta_{\text{conv}} \cdot \eta_{\text{SRM}}. \tag{19}$$

ACKNOWLEDGMENT

The authors would like to thank Panaphase Technologies for funding this paper and helping with manufacturing the prototype machine and for their support in measuring the acoustic noise.

REFERENCES

[1] R. Krishnan, S.-Y. Park, and K. Ha, "Theory and operation of a four-quadrant switched reluctance motor drive with a single controllable switch—The lowest cost four-quadrant brushless motor drive," *IEEE Trans. Ind. Appl.*, vol. 41, no. 4, pp. 1047–1055, Jul./Aug. 2005.

[2] S. Vukosavic and V. R. Stefanovic, "SRM inverter topologies: A comparative evaluation," *IEEE Trans. Ind. Appl.*, vol. 27, no. 6, pp. 1034–1047, Nov./Dec. 1991.

[3] R. Krishnan, *Switched Reluctance Motor Drives*. Boca Raton, FL: CRC Press, 2001.

[4] R. Krishnan and P. N. Materu, "Design of a single-switch-per-phase converter for switched reluctance motor drives," *IEEE Trans. Ind. Electron.*, vol. 37, no. 6, pp. 469–476, Dec. 1990.

[5] J. C. Morse, "Design and implementation of a novel control system for four quadrant operation of a two-phase switched reluctance motor," M.S. thesis, ECE Dept., Virginia Tech, Blacksburg, 2003.

[6] S.-G. Oh and R. Krishnan, "Two phase flux reversal free stator: Concept, analysis, design, and experimental verification," in *Proc. IAS Conf.*, Oct. 2006, pp. 1155–1162.

[7] K. Ha, C. Lee, J. Kim, R. Krishnan, and S.-G. Oh, "Design and development of brushless variable speed motor drive for low cost and high efficiency," in *Proc. IAS Conf.*, Oct. 2006, pp. 1649–1656.

[8] W. Thong and C. Pollock, "Two phase switched reluctance drive with voltage doubler and low dc link capacitance," in *Proc. IEEE IAS Conf.*, 2005, pp. 2155–2159.

[9] S. J. Yang, *Low-Noise Electrical Motors*. Oxford, U.K.: Clarendon, 1981.
[10] P. Vijayraghavan and R. Krishnan, "Noise in electric machines: A review," *IEEE Trans. Ind. Appl.*, vol. 35, no. 5, pp. 1007–1013, Sep./Oct. 1999.
[11] T. R. Kuphaldt, *All about Circuits—Chapter 12. The physics of conductors and insulators—Temperature coefficient of resistance*, vol. 1-DC, 2003. [Online]. Available: www.Allaboutcircuts.com
[12] G. R. Slemon and A. Straughen, *Electric Machines*. Reading, MA: Addison-Wesley, 1980.

Keunsoo Ha (S'04) was born in Seoul, Korea, on February 25, 1970. He received the B.S. and M.S. degrees in electrical and control engineering from Hong-Ik University, Seoul, Korea, in 1993 and 1995, respectively. He is currently working toward the Ph.D. degree at Virginia Polytechnic Institute and State University, Blacksburg.

In 1995, he worked with the Precision Machinery Research Center, Korea Electronics Technology Institute, where he had been a Senior Researcher for two years and researched in developing the brushless dc motor drives for household air-conditioners and refrigerator's fan and step motor controllers for car dashboard and linear motor drivers for machine tools. His research interests include electric motor drives and power electronics, and his principal research concerns the sensorless control of switched reluctance motor.

Mr. Ha was the recipient of the Third Paper Prize Award from the Industrial Drives Committee of the IEEE Industry Applications Society.

Cheewoo Lee (S'05) was born in Busan, Korea, in 1972. He received the B.S. and M.S. degrees in electrical engineering from Pusan National University, Pusan, Korea, in 1996 and 1998, respectively. He is currently working toward the Ph.D. degree at Virginia Polytechnic Institute and State University, Blacksburg.

In 1998, he was with the Digital Appliance Company of LG Electronics Inc., where he had been a Senior Research Engineer since 2002 and has conducted research on the development of Induction Motors, SynRMs, and brushless dc motors for a compressor in home-appliance air conditioners and refrigerators. His research interests include controllable electric motor drives and their optimal control using a DSP.

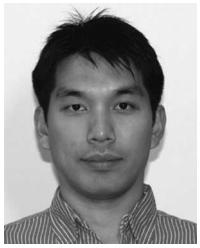

Jaehyuck Kim (S'05) received the B.S. degree in electrical engineering from Hanyang University, Seoul, South Korea, in 1999, and the M.S. degree from University of Wisconsin, Madison, in 2004. He is currently working toward the Ph.D. degree at Virginia Polytechnic Institute and State University, Blacksburg.

From 1999 to 2000, he worked with the Underwriters Laboratory Korea, Ltd., where he was a Field Engineer in the area of the product safety and certification. His primary area of interest is power electronic control of electric motors, specifically, switched reluctance and permanent magnet synchronous motor.

R. Krishnan (S'81–M'82–SM'95–F'01) received the Ph.D. degree in electrical engineering from Concordia University, Montreal, QC, Canada.

He is a Professor of electrical and computer engineering at Virginia Polytechnic Institute and State University, Blacksburg. His research interests are analysis, design and innovations in electric motor drives, electric machines, and power converters for motor drives and applied control. He is the author of *Electric Motor Drives* (Prentice Hall, Feb. 2001), its Chinese translation (Pearson Education Taiwan, 2002), Indian Edition (Prentice Hall of India, 2002), and International Edition (Prentice Hall International Edition, 2001), and the author of *Switched Reluctance Motor Drives* (CRC Press, June 2001) (first edition) and 2003 (second edition), and Coeditor of *Control in Power Electronics* (Academic Press, Aug. 2002). He directs the Center for Rapid Transit Systems pursuing unique, safe, high-speed, energy efficient, and personal electric transit solutions. He has been a Consultant for more than 18 companies in USA. He has developed and delivered short courses for industry on vector-controlled induction motor drives, permanent magnet synchronous and brushless dc motor drives, switched reluctance motor (SRM) drives, and linear electric motor drives. His inventions constituted the founding technologies for two start-up companies in the U.S. in linear and rotating SRM drives technologies, respectively. Apart from founding these companies, he served as the founding Chief Technical Officer for some time to both. He has been granted three U.S. patents, and many are pending in U.S., Europe, and other countries. His inventions have been prominently featured in public media, including radio, TV, and newspapers such as *The Wall Street Journal*.

Mr. Krishnan was the recipient of Four Best Paper Prize Awards from IEEE Industry Applications Society Industrial Drives committee. His coedited book *Control in Power Electronics* won the Best Book Award from Ministry of Education and Sport, Poland, in 2003. In addition, he received the first prize from the IEEE TRANSACTIONS ON INDUSTRY APPLICATIONS for his paper. He is a Fellow of the IEEE cited for his contributions to the development of ac and SRM drives. He was also the recipient of IEEE Industrial Electronics Society's Dr. Eugene-Mittelmann Achievement Award for Outstanding Technical Contributions to the Field of Industrial Electronics. He is a Distinguished Lecturer of IEEE Industrial Electronics Society. He is an elected Senior AdCom Member of IEEE Industrial Electronics Society and served as Vice President (publications) from 2002 to 2005. He served as the General Chair of the 2003 IEEE Industrial Electronics Conference, Roanoke, VA, and as one of the three General Co-Chairs of the IEEE Industrial Electronics Society International Conference on Industrial Technology 2006 in Mumbai, India.

Seok-Gyu Oh (S'93–M'98) was born in Korea in 1967. He received the B.S., M.E., and Ph.D. degrees in electrical engineering from Pusan National University, Pusan, Korea, in 1991, 1993, and 1997, respectively.

He was an Engineer with Hyundai Heavy Industries from 1993 to 1994. He has been with Jinju National University, Jinju, Korea, as an Associate Professor in the Department of Mechatronics Engineering since 1998. He was a Visiting Professor in the Department of Electrical and Computer Engineering, Virginia Polytechnic Institute and State University, Blacksburg, from 2004 to 2006. His current research interests are motor design and control of motor using power electronics.